Trans Indian Inst Met (2019) 72(4):849–857
https://doi.org/10.1007/s12666-018-1541-3

TECHNICAL PAPER

Effect of Recovery and Recrystallization on the Damping Behaviour of A356/SiC_p Composites

M. S. Bhaskar[1] · **M. K. Surappa**[2]

Received: 14 March 2018 / Accepted: 14 December 2018 / Published online: 4 January 2019

Abstract Damping characteristics of A356 alloy and its composites reinforced with 15 vol% SiC particles were investigated using a dynamic mechanical analyzer. Tests were done at three different temperatures 150 °C, 200 °C and 300 °C to study the influence of microstructural changes during recovery and recrystallization on the damping behaviour. Since recovery and recrystallization also depend on the heating rate, damping tests were done at slow (2 °C/min) and fast (10 °C/min) heating rates. The damping characteristics were explained with respect to the microstructure changes that took place during recovery and recrystallization.

Keywords Metal-matrix composites · Damping · Casting · Extrusion

1 Introduction

Aluminium matrix composites based on A356 (Al–7Si–0.3Mg) have been studied elaborately. These composites are used as rotors/discs in braking system. Investigations so far have focused on understanding the ageing behaviour [1–5]; casting and deformation processing [6–8] and sliding wear properties [9–12]. Mechanical vibration causes much damage in automotive industries. So it is important to seek for high damping capacity materials to eliminate such damage. Metal-matrix composites (MMCs) are promising materials for applications requiring high damping capacity. In MMCs, damping capacity is improved through the addition of reinforcing phases that possess high intrinsic damping or by the modification of the matrix microstructure by the reinforcement. Zhang et al. [13] enumerated the entire damping mechanisms operative in MMCs. Zhang et al. [14] showed that the damping capacity increased with increase in reinforcement content in Al–$TiAl_3$ composite. This was attributed to the increase in the thermal mismatch generated dislocations. Effect of microstructure modification on the damping behaviour of Mg_2Si/Mg–9Al composites was studied by Li et al. [15]. Chinese script morphology of Mg_2Si was modified using 0.5 wt% Sb. The resultant microstructure contained polygonized Mg_2Si which showed better damping capacity. During forming operations, MMCs may experience appreciable amounts of cold work which may degrade some mechanical properties such as elongation to fracture and fatigue resistance. Lu et al. [16] discussed the effect of cold rolling on the damping ability of 2048Al/SiC composites. It was observed that elastic modulus and damping coefficient were insensitive to the amount of cold work if a good SiC–Al interfacial bond existed. It became necessary to anneal the composite after some forming operations. During annealing, deformed material undergoes recovery and recrystallization. During recovery, the dislocations arrange themselves into a cell structure wherein dislocation-free sub-grains are separated by dislocation walls. During recrystallization, strain-free grains nucleate and grow in the deformed matrix. Zhang et al. [17] and Shanta Shastry et al. [18] studied the damping behaviour of

✉ M. S. Bhaskar
metsiva@nitw.ac.in

M. K. Surappa
mirle@iisc.ac.in

[1] Metallurgical and Materials Engineering Department, National Institute of Technology Warangal, Hanamkonda, India

[2] Department of Materials Engineering, Indian Institute of Science, Bangalore, India

Mg/TiC and ZA27/aluminite composites, respectively, as a function of temperature. They suggested that at low temperature, thermal mismatch generated interface dislocations were the main source of damping. At high temperature, interface and grain boundary sliding were the damping sources.

The aim of this work is to understand the influence of changes in microstructure that take place during recovery and recrystallization on the damping behaviour of this composite.

2 Materials and Methods

The composite was produced by melt stir technique [1]. The cast ingot was machined to a billet size of 55 mm diameter × 60 mm length. The billet was hot extruded at an extrusion ratio of 29:1 to 9 mm × 9 mm cross-sectional area rods. Extruded rod was cold rolled to 80% reduction in thickness to a final thickness of 1.8 mm. After rolling, the strips were observed to have a width of 16 mm. Cold-rolled sheet was isothermally annealed at three different temperatures, i.e. 150 °C, 200 °C and 300 °C. Annealing at 300 °C was done in a salt bath furnace. Annealing at 150 °C and 200 °C was conducted in oil-bath furnace. Matrix microhardness was measured using Shimadzu micro-hardness tester. Metallographic specimens were fine polished up to 2500 grit emery paper. After this, cloth polishing was done using 0.3 μm α alumina suspension. Microstructure was examined in Carl Zeiss optical microscope and Quanta SEM-based EBSD (electron backscattered diffraction). Samples for EBSD were electropolished using Struers electro polishing machine. *I*–2θ XRD (X-ray diffraction) scans were done on Pan Analytical XRD. Damping measurements were done using GABO Eplexor DMA. The samples were machined from the rolled sheet. Sample dimensions were 45 mm × 5 mm × 1.6 mm. Samples were loaded in a three-point bending arrangement, and the loss tangent (tanφ) and elastic modulus were recorded. All the tests were conducted at a frequency of 5 Hz.

3 Results

As seen from Fig. 1, SiC is uniformly distributed. However, particles of varied sizes are seen. Eutectic Si is in the modified form. There is no porosity seen. The volume fraction of SiC added is 15%.

3.1 Hardness

Figure 2 shows the hardness versus holding time for the three annealing temperatures. From Fig. 2, it can be

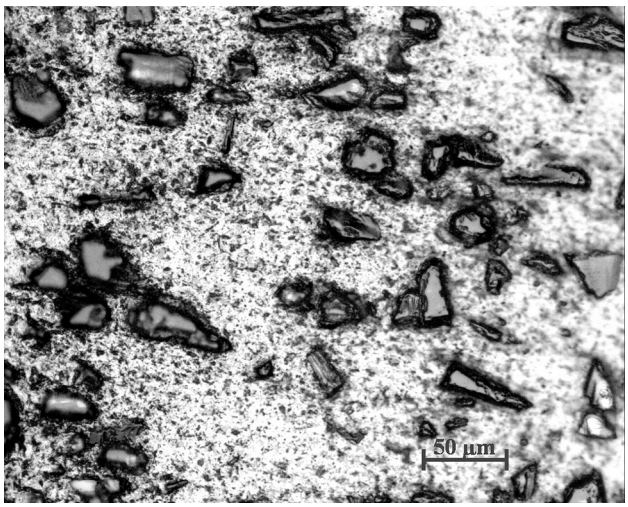

Fig. 1 Optical micrograph of A356/SiC_p composite in the hot-extruded condition

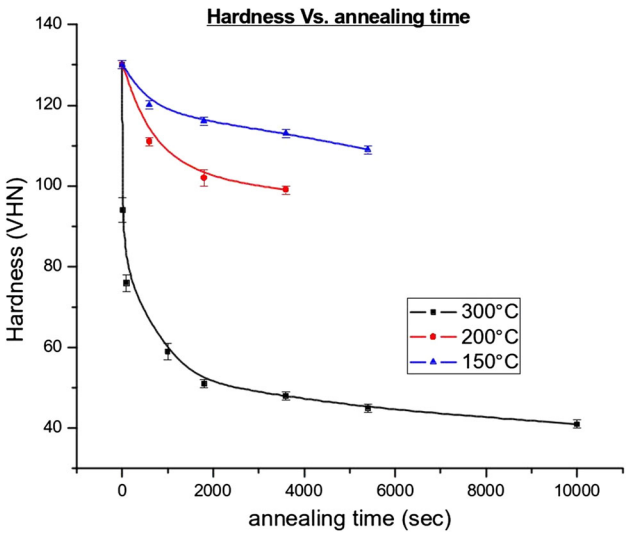

Fig. 2 Hardness versus annealing time at the three holding temperatures

observed that the Vickers hardness number (VHN) in the cold-rolled condition is 130. During annealing at 300 °C, there is a steep drop in hardness. In less than 15 min time, the hardness reduces by 50%. After annealing for 30 min, the hardness levels off. Going by the norm of reduction in hardness alone, one may expect a complete recrystallization or even grain growth after annealing for 10,000 s. But after 10,000 s, the composite is found to be only 40% recrystallized and no grain growth has taken place as revealed from EBSD patterns. The decrease in hardness due to annealing at 150 °C is less. After annealing for 90 min, the hardness decreases to 109VHN. Judging by this decrease in hardness, the softening due to annealing at 150 °C can be attributed to recovery alone. Annealing at 200 °C for 1 h results in a decrease in hardness to 99 VHN.

Recovery and to some extent recrystallization should be operative during annealing.

3.2 EBSD Micrographs

EBSD micrographs have been taken in order to correlate the microstructure with the damping behaviour (Sect. 3.4).

As seen from Fig. 3, the starting grain size is very coarse, typically 0.8 mm elongated in the extrusion direction. The grains are strain free as we can see a clear pattern. The unindexed points (black) correspond to SiC particles. The inverse pole figure seen in Fig. 3 is also applicable from Figs. 4, 5, 6 and 7b with reference to crystallographic orientation.

Cold rolling to 80% reduction in thickness leads to grain fragmentation (dark areas in Fig. 4), and there appears to be S texture component, i.e. {123} ‖ rolling plane and <634> ‖ rolling direction. Grain size after cold work is 6 μm. Since the aim of our paper is to study the damping behaviour of the composite, going forward we shall discuss the EBSD micrographs only with respect to observed grain morphologies and not the textures developed.

From Fig. 5, i.e. EBSD micrograph for annealing at 150 °C for 60 min, we can see a gradual change in orientation as compared to the cold-rolled condition. This is a sign of recovery wherein a prior deformed grain develops sub-grains having different orientations. The sub-grain boundaries are low angle. So the orientation change across the grains is small.

The banded structure that is seen at 150 °C is also seen at 200 °C as seen from Fig. 6. So it is predominantly recovery that take place at these two temperatures. But at the end of 60 min for annealing at 200 °C, there is some recrystallization which can be seen from the microstructure. Annealing at 300 °C produces prominent recrystallization as seen in Fig. 7a (annealing for 1000 s) and b (annealing for 10,000 s).

3.3 Dislocation Density

Figures 8 and 9 show the *I* versus 2 plot (obtained from X-ray diffraction) after annealing at 150 °C and 300 °C, respectively. From Figs. 8 and 9, it can be seen that even though there is 15% SiC present in the material (confirmed through optical microscopy, e.g. Figure 1), we are mostly

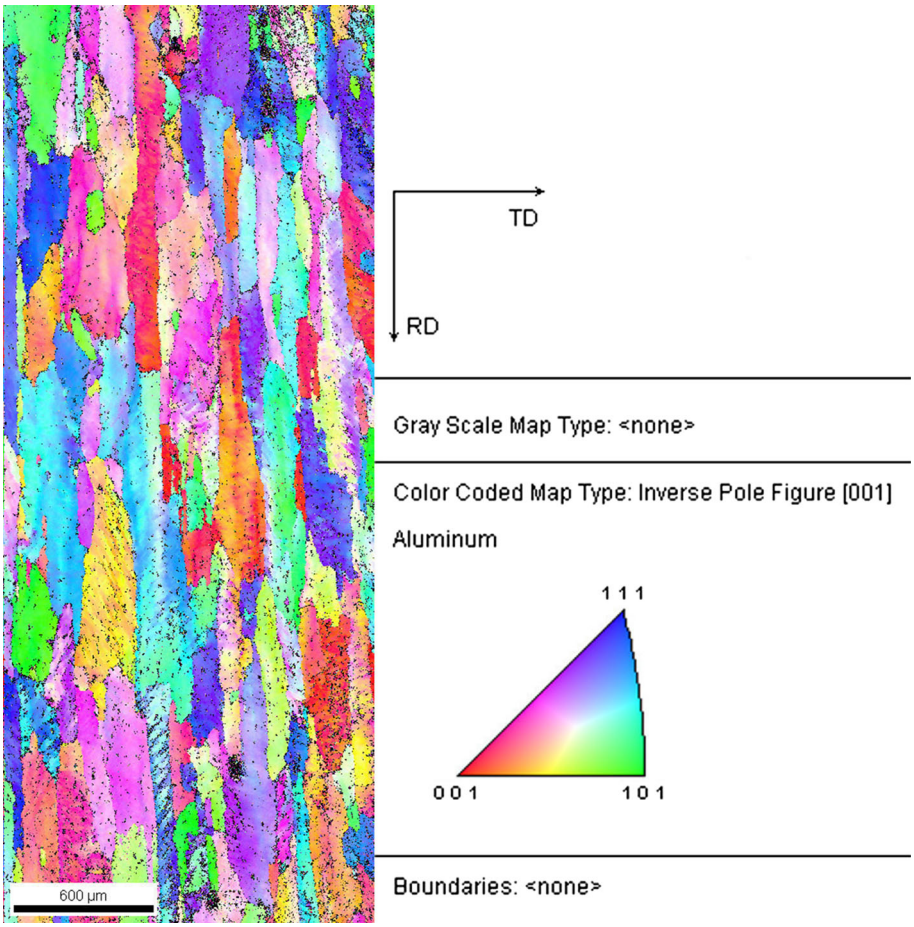

Fig. 3 EBSD micrograph of the composite in the hot-extruded condition showing coarse elongated grains in the extruded direction

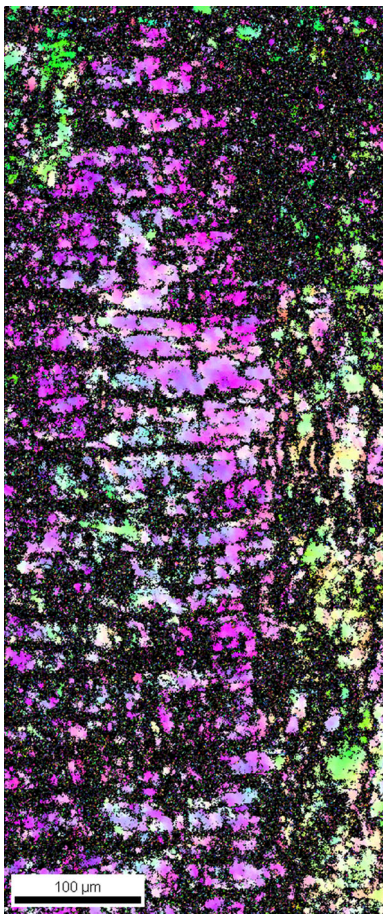

Fig. 4 EBSD micrograph after cold rolling to 80% reduction in thickness

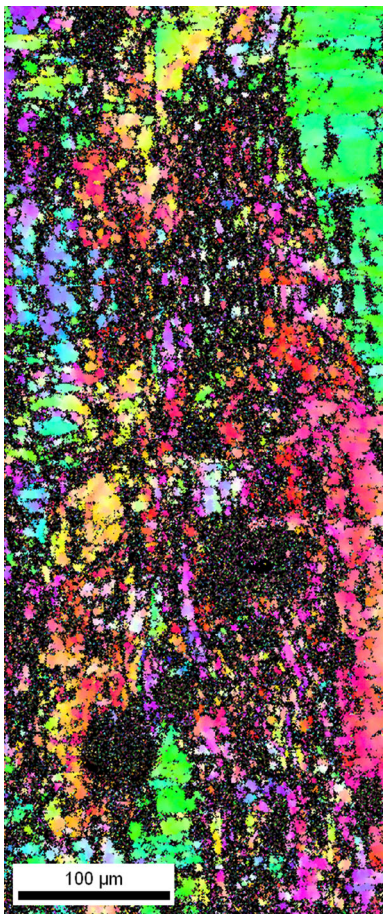

Fig. 5 EBSD micrograph after annealing the cold-rolled composite at 150 °C for 60 min

finding FCC matrix peaks in the XRD pattern. Dislocation densities have been calculated from the XRD peak profiles (taken from I vs. 2θ scans) following Groma et al. [19]. Figure 10 shows the variation of dislocation density with isothermal annealing at 150 °C and 300 °C. From Fig. 10, it can be observed that the dislocation density in the cold worked condition is 1.43×10^{16} m^{-2}. The dislocation density decreases slightly up to 60 min while annealing at 150 °C. Thereafter, it decreases and reaches a value of 2.24×10^{9} m^{-2} after 90 min of annealing at 150 °C. The decrease in the dislocation density at 150 °C suggests that the operating softening mechanism is recovery. From Fig. 10, it can also be observed that there is a noticeable decrease in the dislocation density after annealing for 100 s. After annealing for 1000 s at 300 °C, the decrease is substantial, i.e. to 10^{10} m^{-2} and stays same even after longer periods of anneal.

This suggests that recrystallization has taken place around 1000 s.

3.4 Damping

Material damping is a property related to time-dependent elasticity. Defects are the most important source of damping. Damping results from the internal friction exerted on atomic movement in regions of defects. Defects introduce stress concentration in the crystal. Although applied stress is well below yield stress, the internal stress concentration in regions of high defect density atomic rearrangement can take place. At ambient temperature, the relative atomic displacements are fractions of atomic diameter. At high temperatures, sliding can be extensive leading to visco-elastic strain. These displacements cause internal relaxation and can be recovered upon removal of load. This phenomenon in cyclic loading leads to mechanical hysteresis in stress versus strain behaviour. Lavernia et al. [20] reviewed the damping behaviour of aluminium matrix composites. Damping properties are analysed using dynamic mechanical analyzer (DMA). The key parameter which characterizes a material's damping behaviour is the damping coefficient. Damping coefficient is defined as tan(φ) where φ is the loss angle or phase lag

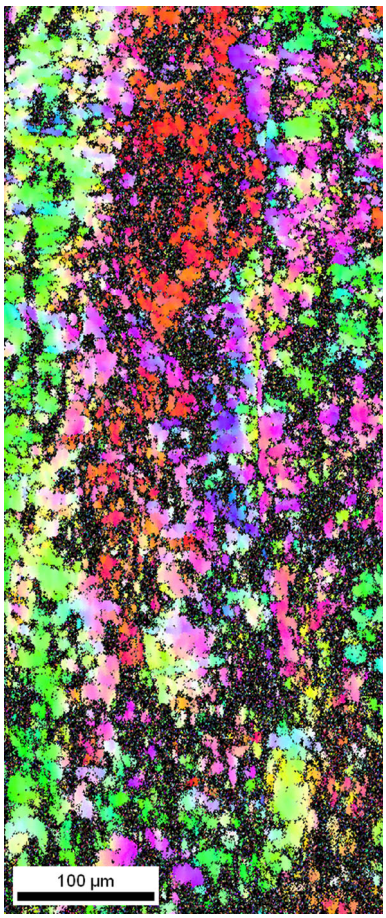

Fig. 6 EBSD micrograph after annealing the cold-rolled composite at 200 °C for 60 min

between sinusoidally applied stress and the observed strain [20]. A higher value of tan(φ) indicates a better damping behaviour.

The properties measured for the alloy at room temperature using DMA are:

$$\text{Dynamic modulus} = 64.11 \pm 0.35 \text{ GPa}$$
$$\text{Damping coeffcient} = 0.034 \pm 0.002$$

The properties for the composite at room temperature are found to be:

$$\text{Dynamic modulus} = 83.77 \pm 0.34 \text{ GPa}$$
$$\text{Damping coeffcient} = 0.032 \pm 0.001$$

From the measurements, we can see that the composite has better modulus than the base alloy but the damping coefficients of both alloy as well as composites are comparable at room temperature. Time sweep, i.e. subjecting the material to cyclic loading at a given temperature, has been conducted to evaluate the damping behaviour of composites vis-a-vis alloys at high temperatures. Isothermal annealing can lead to relaxing

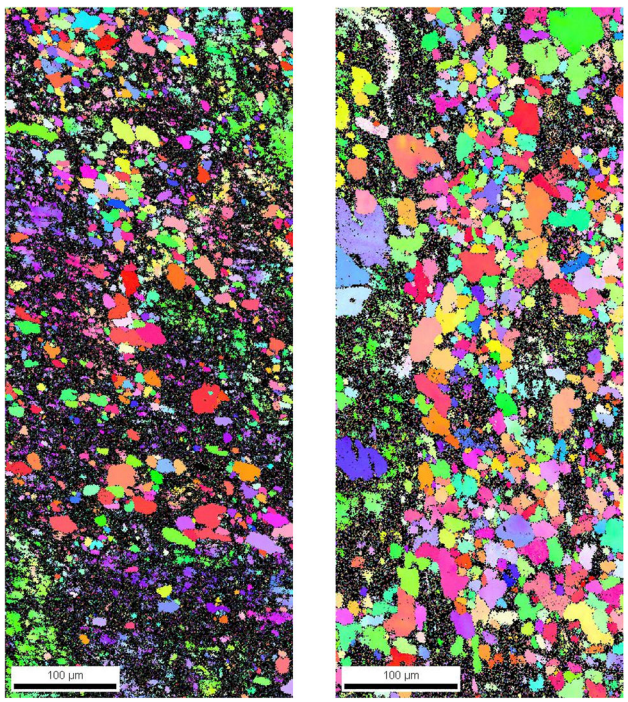

Fig. 7 EBSD micrograph of the composite after annealing at 300 °C

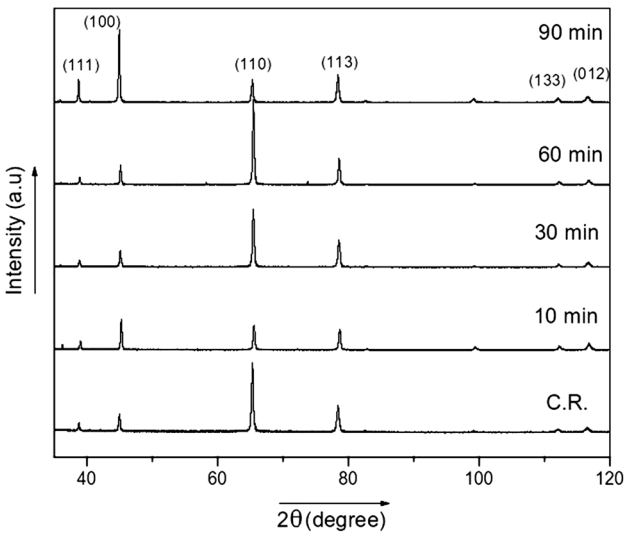

Fig. 8 Intensity versus 2θ plot for composite annealed at 150 °C

phenomena such as recovery and recrystallization, which in turn results in changes in substructure. Damping characteristics are an indirect indication of these changes.

From Fig. 11, we can see that with increase in annealing time, there is negligible change in elastic modulus (E) of alloy. For composite, the tests have run up to a maximum time of 25 min. Pre-existing weak sites such as edge cracks (which has happened during cold rolling) are the cause of

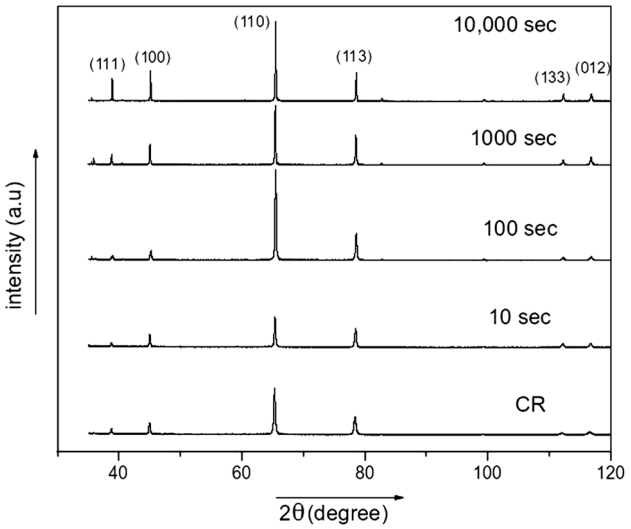

Fig. 9 Intensity versus 2θ plot for composite annealed at 300 °C

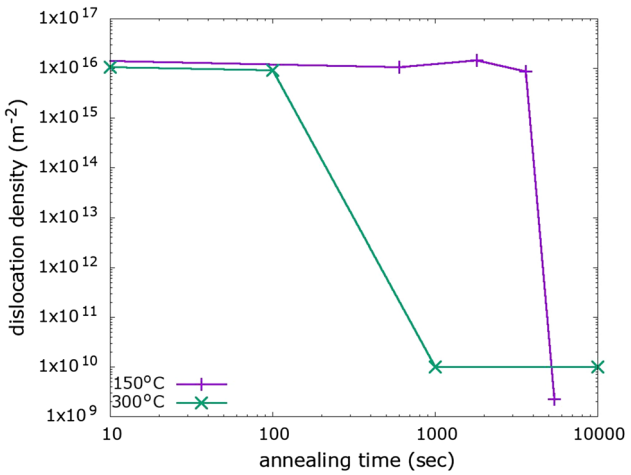

Fig. 10 Dislocation density versus annealing time when the composite is annealed at 150 °C and 300 °C

this failure. There is a moderate increase in the E of composite with time. EBSD patterns (Fig. 5) suggest recovery to happen during this time interval. Although recovery is a softening mechanism, we see a clear, but mild increase in elastic modulus during isothermal ageing at 150 °C. We believe that this phenomenon needs further investigation in order to establish the causes for the aforementioned phenomena. Damping coefficients of alloy and composite at 150 °C are more or less identical.

Figure 12 shows the time sweep at 200 °C. From Fig. 12, it can be seen that the modulus of composite initially decreases and then increases with time. Modulus of alloy is less than that of composite, and its rate of increase with annealing time is found to be less when compared to the composite. Up to 1 h, the damping capacity of the composite is lower than that of the alloy. But after 1 h, the composite exhibits better damping with increase in time. It is significantly high at 90 min annealing time (i.e. tan $\varphi = 0.09$). As recovery proceeds, the grains rearrange into dislocation-dense walls and dislocation-free sub-grains. In a recovered structure, the vibration amplitude of the dislocation string (*G–L* theory) is higher as there is no tangle formation by interaction with other dislocations. This leads to enhanced damping at this temperature.

From Fig. 13, it can be seen that while annealing at 300 °C, modulus of the alloy doesn't change much with time, whereas there is a moderate increase in modulus for composite. Modulus of composite is higher than that of the alloy. The change in damping coefficient for alloy is relatively less when compared to the composite during the course of annealing. For the composite, damping coefficient drops initially up to 15 min and then rises to almost double that of the starting value at the end of annealing time of 100 min. Decrease in the dislocation density due to recrystallization, as seen in Fig. 7b, is responsible for the observed increase in damping coefficient of the composite. One of the damping mechanisms which are more pronounced in the case of the composite, i.e. interface damping (at the matrix/particle interfaces), also becomes more active at high temperatures. The notable increase in the damping coefficient of the composite compared to the alloy suggests interface damping to be prominent mechanism after 60 min.

Heating rate can influence the relative span of relaxation mechanisms. This can in turn influence the final microstructure. This signature of the microstructure (or substructure) change can also be studied by observing the damping behaviour. In order to study the relative efficacy of fully recovered microstructure versus a fully recrystallized microstructure, damping phenomena in our composite (and the base metal, for comparative purposes) have been studied at two heating rates, 2 °C/min and 10 °C/min.

From Fig. 14, we find that the alloy shows lower modulus than composite all throughout the test, i.e. heating rate of 2 °C/min. Modulus decreases with increase in temperature. After 230 °C, there is large softening of the alloy and the elastic modulus drops steeply. There is no such decrease observed in the composite. The reinforcement content is responsible for the sustained modulus. Damping coefficient of the composite is much higher than that of the alloy. Up to 200 °C, the main damping contribution is from the thermal mismatch induced dislocations. After 200 °C, their contribution to the overall damping reduces as misfit strain decreases with increase in temperature. The main

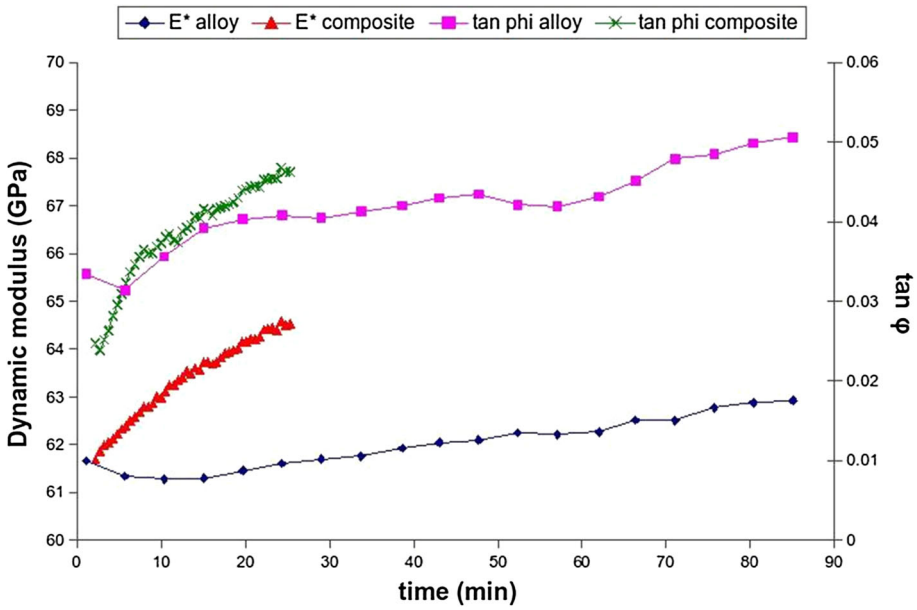

Fig. 11 Time sweep at 150 °C

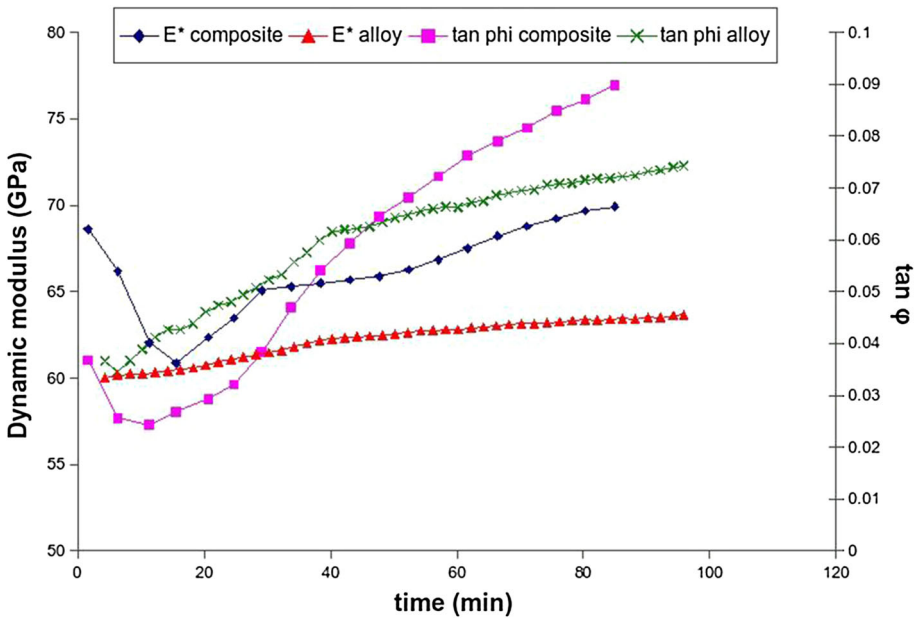

Fig. 12 Time sweep at 200 °C

damping mechanisms after 200 °C are viscous sliding of interfaces and grain boundaries. Presence of the damping peak at 185 °C for composite and 200 °C for the alloy is due to the avalanche effect of unpinning of dislocations, i.e. as the testing temperature increases, dislocation string breaks away from the weak pinning and unpinning of dislocation occur. After 220 °C, the pronounced increase in the damping of the composite which is absent in the alloy suggests that interface damping is a very important component to damping at these temperatures.

From Fig. 15 we observe that while heating at 10 °C/min, composite fails at fairly low temperature, i.e. 160 °C. The modulus first increases with temperature up to 65 °C and then it decreases. The decrease in modulus is very steep. On the other hand, for the alloy, the sample is sound up to 355 °C. The decrease in modulus is not as steep as

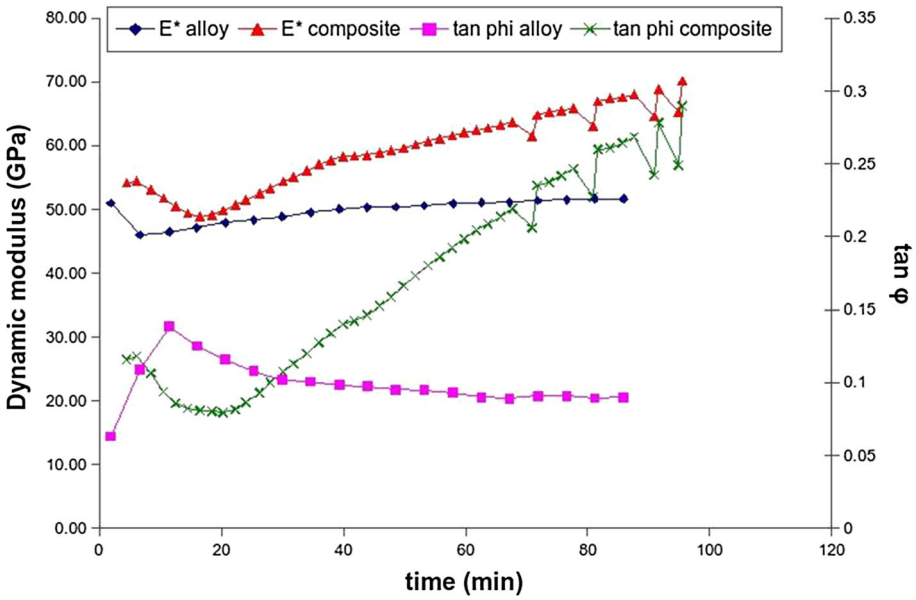

Fig. 13 Time sweep at 300 °C

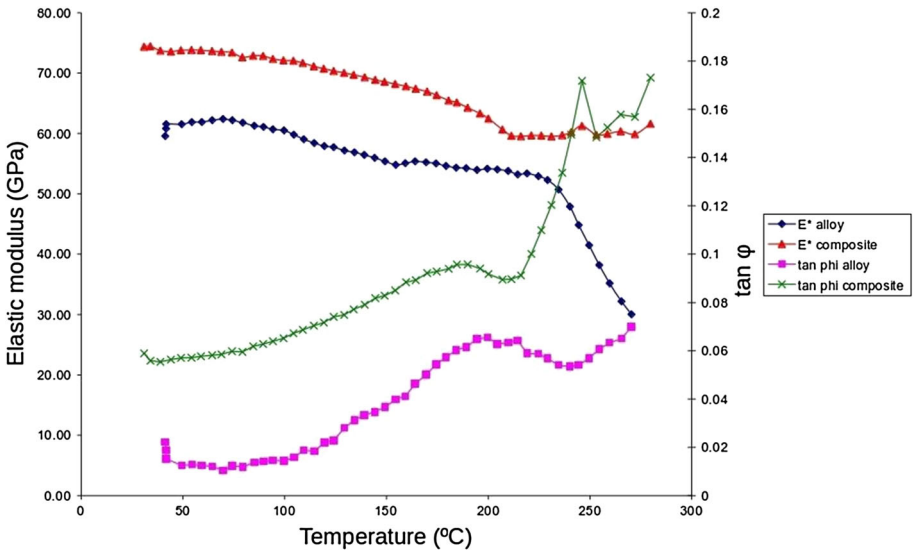

Fig. 14 Temperature sweep at 2 °C/min

that of composite. The alloy when heated at 10 °C/min shows a similar damping behaviour as the one heated at 2 °C/min. The first peak in the damping curve appears at 230 °C. This corresponds to the avalanche effect of unpinning of dislocations. There is a second peak of the damping curve of alloy arising due to the viscous sliding at the grain boundaries and interfaces.

4 Conclusions

From our study, we find that A356/SiC_p composite exhibits better damping than the base alloy, especially at high temperatures. This is due to the enhanced damping contribution coming from particle/matrix interfaces at high temperatures. Recovery and recrystallization bear their

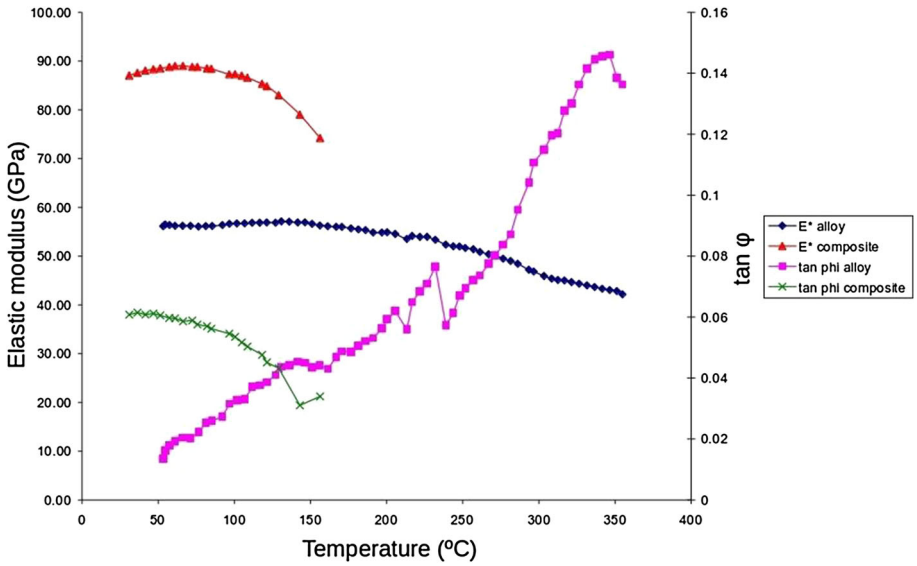

Fig. 15 Temperature sweep at 10 °C/min

signature on the damping response of the composite. The damping peaks, corresponding to the avalanche effect of dislocation unpinning and the grain boundary and interface sliding, are observed earlier in the composite.

References

1. Stephens J J, Lucas J P, and Hosking F M, *Scr Metall* **22** (1988) 1307.
2. Bayoumi M A, Ribes R, and Suery M, Aging characteristics of Sic-particle reinforced Al-Si alloy, in *Proceedings of 9th International Symposium in Metallurgy and Materials Science, Riso, Denmark*, vol 8, p 291 (1988).
3. Kumai S, Hu J, Higo Y, and Nunomura S, *Scr Metall Mater* **27** (1992) 107.
4. Cottu J P, Couderc J J, Viguier B, and Bernard L, *J Mater Sci* **27** (1992) 3068.
5. Salvo L, L'Esprance G, Sury M, and Legoux J G, *Mater Sci Eng A* **177** (1994) 173.
6. Samuel A M and Samuel F H, *Metall Trans A* **24** (1993) 1857.
7. Wang Z and Zhang R J, *Metall Trans A* **22** (1991) 1585.
8. Rozak G A, Lewandowski J J, Wallace J F, and Altmisoglu A, *J Compos Mater* **26** (1993) 2076.
9. Alpas A T and Zhang J, *Scr Metall Mater* **26** (1992) 505.
10. Alpas A T and Zhang J, *Wear* **155** (1992) 83.
11. Wood J V, Davies P, and Kellie J L F, *Mater Sci Technol* 9 (1993) 833.
12. Garca-Cordovilla C, Louis E, Narciso J, and Pamies A, *Mater Sci Eng A* **189** (1994) 219.
13. Zhang J, Perez R J, Wong C R, and Lavernia E J, *Mater Sci Eng R Rep* **13** (1994) 325.
14. Zhang Y, Ma N, Li X, and Wang H, *Mater Des* **29** (2008) 1057.
15. Zhang X, Liao L, Ma N, and Wang H, *Compos Part A Appl Sci Manuf* **37** (2006) 2011.
16. Lu Y X, Lee C S, Li R K Y, and Lai J K L, *J Mater Process Technol* **91** (1999) 215.
17. Xiuqing Z, Haowei W, Lihua L, and Naiheng M, *Compos Sci Technol* **67** (2007) 720.
18. Sastry S, Krishna M, and Uchil J, *J Alloys Compd* **314** (2001) 268.
19. Groma I and Szekely F, *J Appl Crystallogr* **33** (2000) 1329.
20. Lavernia E J, Perez R J, and Zhang J, *Metallur Mater Trans A* **26** (1995) 2803.